

Engineering Phase Competition Between Stripe Order and Superconductivity in $\text{La}_{1.88}\text{Sr}_{0.12}\text{CuO}_4$

J. Küspert,^{1,*} I. Bialo,^{1,2} R. Frison,¹ A. Morawietz,¹ L. Martinelli,¹ J. Choi,³ D. Bucher,¹ O. Ivashko,⁴ M. v. Zimmermann,⁴ N. B. Christensen,⁵ D. G. Mazzone,⁶ G. Simutis,⁷ A. A. Turrini,⁶ L. Thomarat,^{7,8} D. W. Tam,⁶ M. Janoschek,^{1,7} T. Kurosawa,⁹ N. Momono,^{9,10} M. Oda,⁹ Qisi Wang,^{1,11,†} and J. Chang¹

¹*Physik-Institut, Universität Zürich, Winterthurerstrasse 190, CH-8057 Zürich, Switzerland*

²*AGH University of Krakow, Faculty of Physics and Applied Computer Science, 30-059 Krakow, Poland*

³*Diamond Light Source, Harwell Campus, Didcot OX11 0DE, United Kingdom*

⁴*Deutsches Elektronen-Synchrotron DESY, Notkestraße 85, 22607 Hamburg, Germany*

⁵*Department of Physics, Technical University of Denmark, DK-2800 Kongens Lyngby, Denmark*

⁶*Laboratory for Neutron Scattering and Imaging,*

Paul Scherrer Institut, CH-5232, Villigen-PSI, Switzerland

⁷*Laboratory for Neutron and Muon Instrumentation,*

Paul Scherrer Institut, CH-5232 Villigen PSI, Switzerland

⁸*École normale supérieure Paris-Saclay, 91190 Gif-sur-Yvette, France*

⁹*Department of Physics, Hokkaido University, Sapporo 060-0810, Japan*

¹⁰*Department of Applied Sciences, Muroran Institute of Technology, Muroran 050-8585, Japan*

¹¹*Department of Physics, The Chinese University of Hong Kong, Shatin, Hong Kong, China*

ABSTRACT

Unconventional superconductivity often couples to other electronic orders in a cooperative or competing fashion. Identifying external stimuli that tune between these two limits is of fundamental interest. Here, we show that strain perpendicular to the copper-oxide planes couples directly to the competing interaction between charge stripe order and superconductivity in $\text{La}_{1.88}\text{Sr}_{0.12}\text{CuO}_4$ (LSCO). Compressive c -axis pressure amplifies stripe order within the superconducting state, while having no impact on the normal state. By contrast, strain dramatically diminishes the magnetic field enhancement of stripe order in the superconducting state. These results suggest that c -axis strain acts as tuning parameter of the competing interaction between charge stripe order and superconductivity. This interpretation implies a uniaxial pressure-induced ground state in which the competition between charge order and superconductivity is reduced.

INTRODUCTION

Electronic phases may coexist microscopically, either in a collaborative or competing manner. In elementary chromium, for example, spin and charge density wave orders collaboratively coexist with commensurate ordering vectors [1–3]. A similar spin-charge intertwined order is found in doped lanthanum-based (La-based) cuprate superconductors [4–8]. Competing interaction is often

found in the context of unconventional superconductivity. For example, in kagome metals [9, 10], pnictides [11–13], and heavy Fermion systems [14], superconductivity can be optimized through the suppression of charge or spin density wave orders.

However, an interplay between density waves and superconductivity – at least theoretically – can lead to a collaborative state. This state would be characterized by a spatially modulated Cooper pair density with a commensurate wave vector. Extensive experimental and theoretical efforts have been devoted to study this novel superconducting state [15]. Theory works have predicted a connection between superconductivity and stripe order through a so-called pair density wave [16]. Signatures of these pair density waves have been reported by scanning tunneling microscopy [17], but direct diffraction evidence is still missing. A general challenge is therefore to switch the coupling between superconductivity and charge order from competing to collaborative. Ideally, an external stimulus would tune the coupling between these two phases.

Here, using high-energy x-ray diffraction, we show how compressive c -axis uniaxial pressure, perpendicular to the copper-oxide planes, enhances stripe order inside the superconducting state of $\text{La}_{1.88}\text{Sr}_{0.12}\text{CuO}_4$ (LSCO), while charge order remains unchanged in the normal state. We furthermore discover that the magnetic field enhancement of charge order inside the superconducting state is dramatically reduced upon compressive c -axis strain application. This observation suggests a correspondingly reduced phase competition. We thus demonstrate that c -axis pressure acts directly on the coupling between charge stripe order and superconductivity.

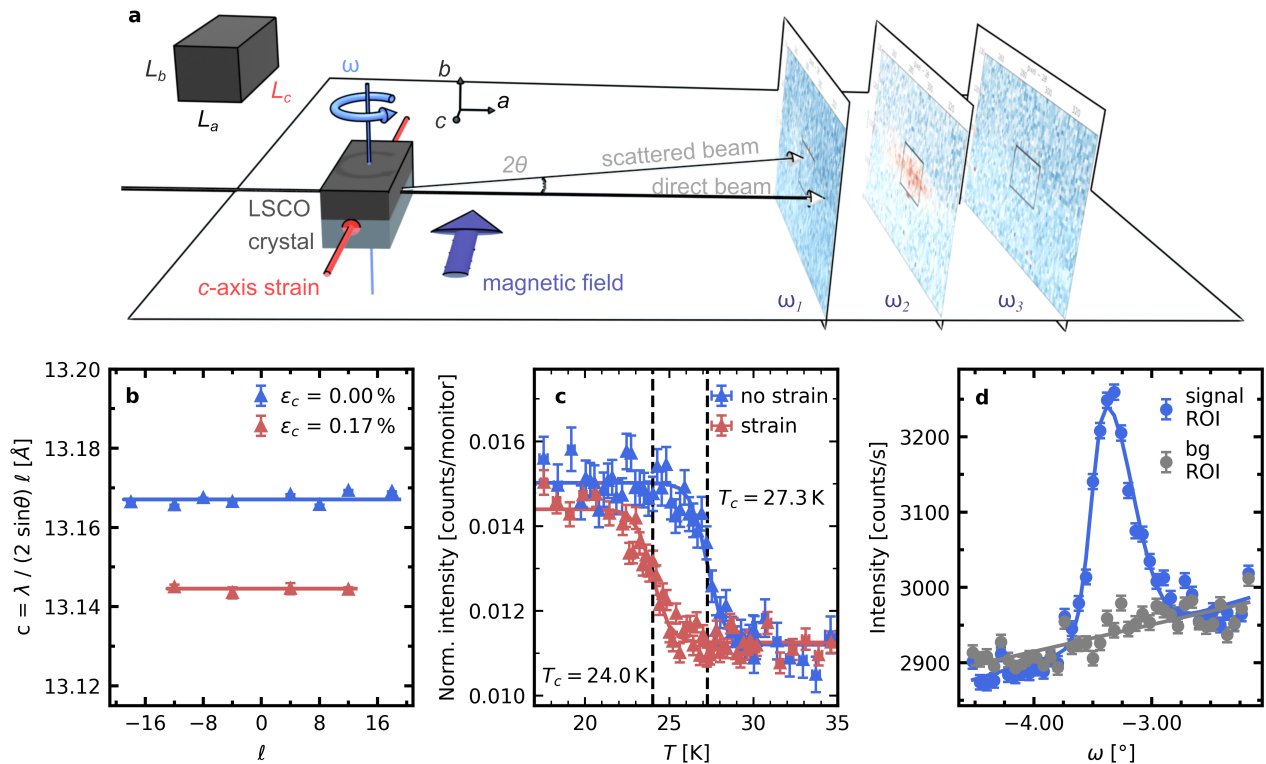


FIG. 1. **Uniaxial pressure application in the hard x-ray diffraction experiment on LSCO.** **a** Schematic illustration of the scattering geometry for high-energy x-ray diffraction on LSCO. Uniaxial pressure and magnetic field are applied along the crystallographic c -axis direction on a cuboid-shaped crystal with dimensions $L_a \cdot L_b \cdot L_c$ as sketched in the top left inset. Detector read-outs with exemplary region-of-interest (ROI, black box in detector images) for three different rotation angles ω around the vertical axis are shown. **b** c -axis lattice parameters, extracted from fits of $(0, 0, \ell)$ Bragg peaks, corresponding to c -axis strains ε_c . Solid lines are least-square fits to $c = \lambda / (2 \sin \omega) \cdot \ell$, where λ is the wavelength of the x-rays. Error bars are standard deviations obtained from the fitting procedure. **c** Spin flip intensities from polarized neutron scattering at $\tau = (-1, -1, 0)$ on LSCO ($T_c = 27$ K), normalized by the monitor and scaled to the integrated Bragg peak intensity of the unstrained measurement. The drop of the curves yields the superconducting transition temperature with and without c -axis uniaxial pressure (see Methods for detailed definition of T_c). **d** Charge order peak at 30 K obtained by integrating the intensities in a region-of-interest (ROI) around $\mathbf{Q}_{co} = (0.231, 0, 12.5)$ (blue points). A background (bg, grey points) is estimated by a similar integration of a ROI slightly shifted off the $(h, 0, \ell)$ scattering plane. Error bars in c and d are dictated by counting statistics.

RESULTS

X-ray Methodology.

Stripe charge order in La-based cuprates manifests itself by weak reflections at $\mathbf{Q}_{co} = \tau + (\delta, 0, 0.5)$ where τ represents fundamental Bragg peaks and $\delta \approx 1/4$ is the stripe incommensurability [6, 7, 18, 19]. We adopted an x-ray transmission geometry with crystalline a - and c -axes spanning the horizontal scattering plane as illustrated in Fig. 1a. Magnetic field and uniaxial pressure were applied along the c -axis direction.

Uniaxial Pressure Application.

The strain as a result of uniaxial c -axis pressure can be directly estimated from lattice parameter measurements. Pressure-induced compression of the c -axis lattice parameter is evidenced by a shift of $(0, 0, n)$ Bragg peaks to

larger scattering angles. Precise strain characterization utilizes multiple such Bragg peaks with n being an even integer (see Method section and Fig. 1b). The resulting c -axis lattice parameter for strained and unstrained LSCO is exemplified in Fig. 1b. As expected, the uniaxial c -axis pressure reduces the c -axis lattice parameter that in turn lowers the superconducting transition temperature T_c [20–22]. Using polarized neutron scattering we confirmed the decrease of T_c with compressive c -axis strain [23–26] – see Fig. 1c and Method section. Exploiting that the lower critical field for superconductivity H_{c1} is low, we track the excess depolarisation of the neutron beam due to flux trapped along the c -axis after field-cooling through T_c . The in-plane polarized neutrons are depolarized by this trapped flux. Upon crossing T_c , the flux is released.

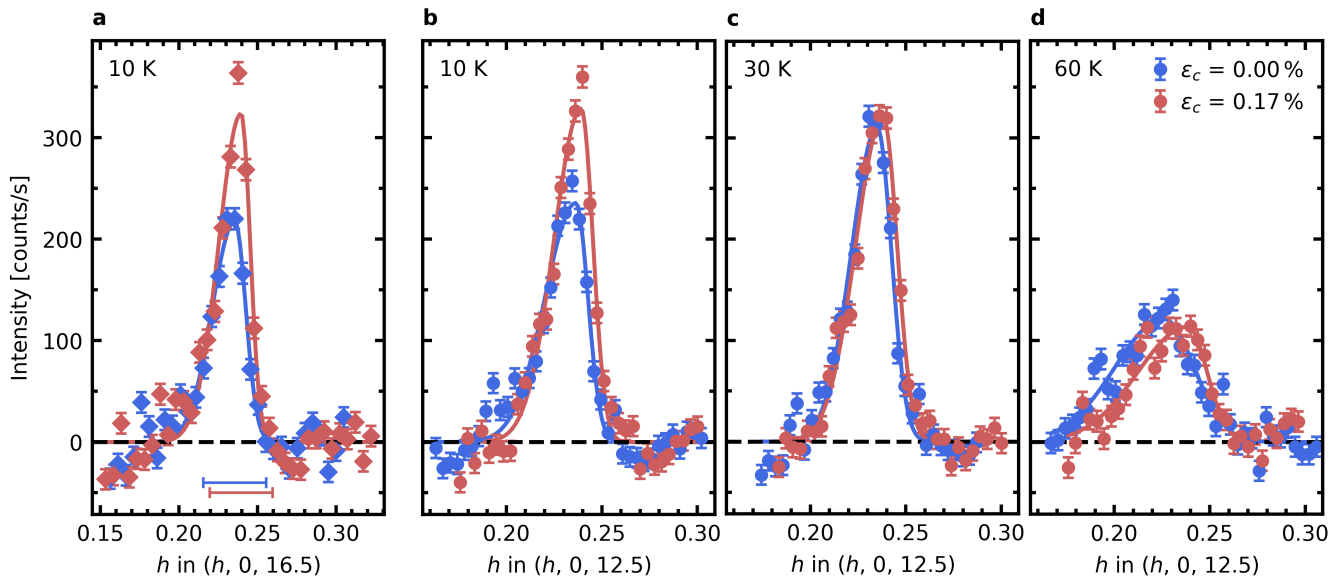


FIG. 2. **Charge order reflection in LSCO upon application of c -axis uniaxial strain.** a-d Background subtracted charge order reflections for temperatures and momenta as indicated. Red (blue) points are recorded with (without) compressive c -axis pressure application. Error bars stem from counting statistics and solid lines are fits with a split-normal distribution including a linear background. The horizontal lines in the bottom of (a) – applying to all panels – represent a systematic error in h stemming from twinning of the sample [27].

Uniaxial c -axis strain effects on charge order.

X-ray diffraction intensity was collected using a two-dimensional single-photon detector. Detector regions-of-interest (ROI) are defined such that the signal or background of interest is covered (see Supplementary Fig. 1). We constructed standard one-dimensional rocking curves (see Fig. 1d for $\mathbf{Q}_{\text{co}} = (\delta, 0, 12.5)$). An advantage of 2D-detectors (over point detectors) is that a background can be estimated by slightly shifting the ROI (grey data in Fig. 1d).

In Fig. 2, we show scans through $\mathbf{Q}_{\text{co}} = (\delta, 0, 12.5)$ and $(\delta, 0, 16.5)$, with and without uniaxial c -axis pressure. Data for a $\text{La}_{2-x}\text{Sr}_x\text{CuO}_4$ crystal with slightly different doping are shown in Supplementary Fig. 2. Intensities and fits are presented after subtracting the background. In the normal state ($T > T_c$), no pressure effect on charge stripe order is observed. Further, we find a significant pressure-induced enhancement of the charge order reflection inside the superconducting state. The correlation length and incommensurability δ remain virtually unaffected by uniaxial pressure. Observed shifts are within the error bars and thus negligible. From here, we therefore consider the charge order peak amplitude as a function of temperature, uniaxial c -axis pressure, and magnetic field. The peak amplitude I_{co} is extracted by fitting intensity profiles with a split-normal distribution on a linear background – see Fig. 1d, 2, Supplementary Fig. 3 and Methods. The temperature dependence of the charge

order amplitude is shown in Fig. 3a for strained and unstrained conditions. In the absence of a magnetic field, compressive c -axis pressure enhances the charge order inside the superconducting state. The charge order peak amplitude, due to phase competition [19], displays a cusp at T_c . The cusp is shifted to slightly lower temperatures upon application of c -axis pressure. Assuming phase competition between charge order and superconductivity, this suggests a reduction of the superconducting transition temperature, in agreement with the measurements in Fig. 1c. At our base temperature ($T = 10\text{ K}$), the relative peak amplitude, $I_{\text{co}}(10\text{ K})/I_{\text{co}}(30\text{ K})$, scales approximately linearly with the applied strain ε_c (see Fig. 3b). Within the examined range of ε_c , the charge order peak amplitude increases by about 25%.

Magnetic field effect.

Without strain, magnetic field effects on charge and spin order inside the superconducting state have already been studied [27, 29–33]. Consistent with previous studies, we find an increase of the charge order amplitude for $T < T_c$ (see Fig. 3c). At base temperature, the charge order intensity scales approximately linearly with magnetic field. At 10 T, the peak amplitude is more than doubled. This is in strong contrast to the ground state reached through application of c -axis pressure. Here, as depicted in Fig. 3d, a much weaker field effect is observed. The magnetic field effect for strained and unstrained conditions is shown in Fig. 3e. Upon increasing strain ε_c , a

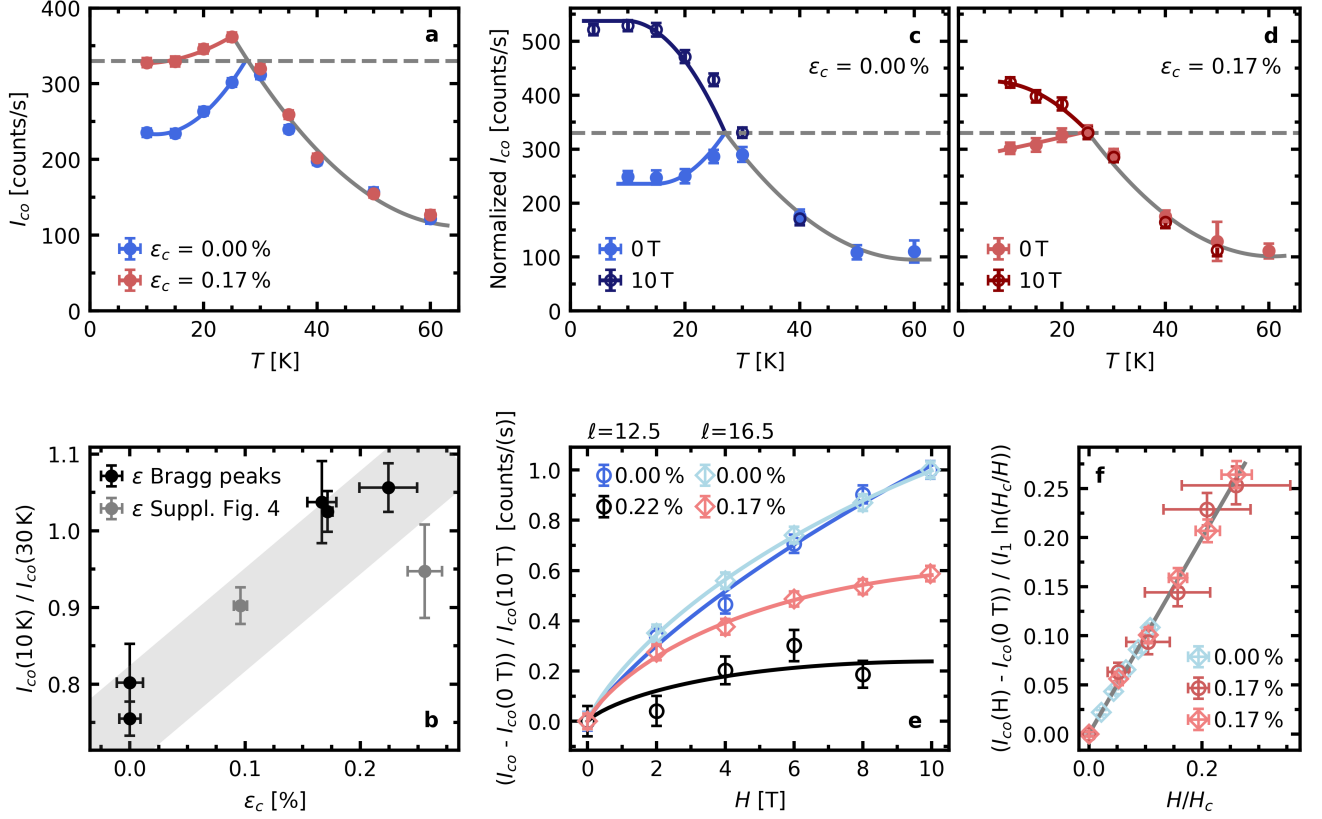


FIG. 3. **Phase competition of charge order and superconductivity.** **a** Temperature dependence of the amplitude I_{co} of the (0.231, 0, 12.5) charge order peak without and with strain measured in a setup without magnetic field. **b** Low-temperature (10 K) charge order amplitude normalized to the normal state (30 K) plotted as a function of c -axis strain. For the black (grey) points, the strains are directly (indirectly) measured. Indirect measurements use the calibration curve in Supplementary Fig. 4. The grey shaded area is a guide to the eye. **c, d** Temperature dependence for charge order peak at (0.231, 0, 12.5) in 0 T and 10 T without and with strain, respectively measured in the cryomagnet. The horizontal dashed lines at $I_{co}(T_c)$ in panels a, c, d serve to facilitate comparison between experiments. **e** Magnetic field dependence at 10 K of the charge order peak amplitude at (0.231, 0, 12.5) (circles) and (0.231, 0, 16.5) (diamonds) for strains as indicated. Solid lines are fits to the data with $I_{co}(\mathcal{H}) = I_{co}(0) + I_1 \mathcal{H} \ln(1/\mathcal{H})$ [28], where $\mathcal{H} = H/H_c$, I_1 is a fitting parameter, and H_c is a critical field scale. **f** Comparison of data obtained with and without strain at (0.231, 0, 12.5) (circles) and (0.231, 0, 16.5) (diamonds) ($T = 10$ K). By application of uniaxial pressure, we roughly double the reachable parameter space in H/H_c . Solid lines in a-c are guides to the eye. The dashed lines indicate the charge order amplitude at T_c and ambient pressure. Error bars are standard deviations from the respective fits.

decreasing magnetic field effect on the charge order intensity is observed inside the superconducting state.

DISCUSSION

There has been an interest to study the stripe order beyond the upper critical field (H_{c2}) for superconductivity [34]. The magnetic field dependence of the charge order amplitude in Fig. 3e is often modelled by $I_{co}(\mathcal{H}) = I_{co}(0) + I_1 \mathcal{H} \ln(1/\mathcal{H})$, where $\mathcal{H} = H/H_c$ and I_1 is a fitting parameter. The critical field scale H_c has been linked to the upper critical field H_{c2} of superconductivity [28]. We however stress that these two field scales (H_c

and H_{c2}) are not necessarily identical. We show in Fig. 3f that we could double the reachable parameter space in \mathcal{H} by applying strain along c . By fitting the observed charge order peak amplitude versus magnetic field, we extract H_c at base temperature (see fitted curves in Fig. 3e). In Fig. 4a, we plot H_c versus strain ϵ_c . The field scale H_c seems to scale approximately linearly with c -axis strain: $H_c = H_c(0) - \alpha \epsilon_c$ with α being a constant. By extrapolation, our results suggest that there exists a critical c -axis strain at which $H_c \rightarrow 0$. At this critical strain $\epsilon_{crit} = H_c(0)/\alpha \approx 0.3\%$, the magnetic field effect is expected to vanish.

Outlining our findings, we illustrate schematically in Fig. 4b the charge order peak amplitude versus magnetic

field and c -axis strain inside the superconducting state. The region with highest intensities is found at high magnetic fields and low strains. The strength of the magnetic field effect depends on the uniaxial strain along c . At the highest applied c -axis strain, the magnetic field effect is strongly reduced. Typically, magnetic field effects inside the superconducting state are interpreted in terms of (i) vortex physics [35, 36] or (ii) phase competition. The vortex density and volume increase with increasing magnetic field strength. It is however difficult to explain the strain-field effects in terms of vortices alone. Within the framework of vortex physics [35, 36], the magnetic field induces normal state vortices. The field-enhanced charge order may then stem from real-space volume increase. However, we see that in zero-field, c -axis strain enhances the charge order peak amplitude. This strongly suggests that vortex physics alone cannot account for the observed phenomenology. Even in the high-magnetic field state where vortices are present, it is not obvious how to explain the strain effect without also involving phase competition.

Reduced (absence of) magnetic field effect would imply either that one phase is partially suppressed (absent) or that the competing interaction is weakened. As no pressure effect is found in the normal state, charge order itself is inert to c -axis pressure. On the other hand, superconductivity is known to be weakened by increasing compressive c -axis pressure [37]. One commonly accepted explanation is that compressive c -axis pressure reduces the apical oxygen distance to the CuO_2 layers. This change of crystal field environment, in turn, boosts the hybridization of $d_{x^2-y^2}$ and d_{z^2} orbitals [38, 39]. Theoretically, such hybridization is expected to be unfavorable for d -wave superconductivity [40, 41]. Therefore, c -axis pressure diminishes the superconducting order parameter. However, there is no evidence of superconductivity being completely suppressed upon moderate pressure along the c -axis [20, 23]. Superconductivity and charge order are therefore expected to coexist. Our results thus suggest a pressure-induced ground state in which the phase competition between charge order and superconductivity is reduced.

METHODS

Crystal Growth and Characterization

Our $\text{La}_{2-x}\text{Sr}_x\text{CuO}_4$ single crystals were synthesised using the traveling solvent floating zone method. The growths were carried out in a 2.0 atm oxygen pressure. Post-growth annealing was carried out in an 800 degree oxygen atmosphere for 100 hours. For a very similar growth recipe, superconducting volume fractions were systematically studied using magnetization and specific heat [42]. In our study, we used single crystals from

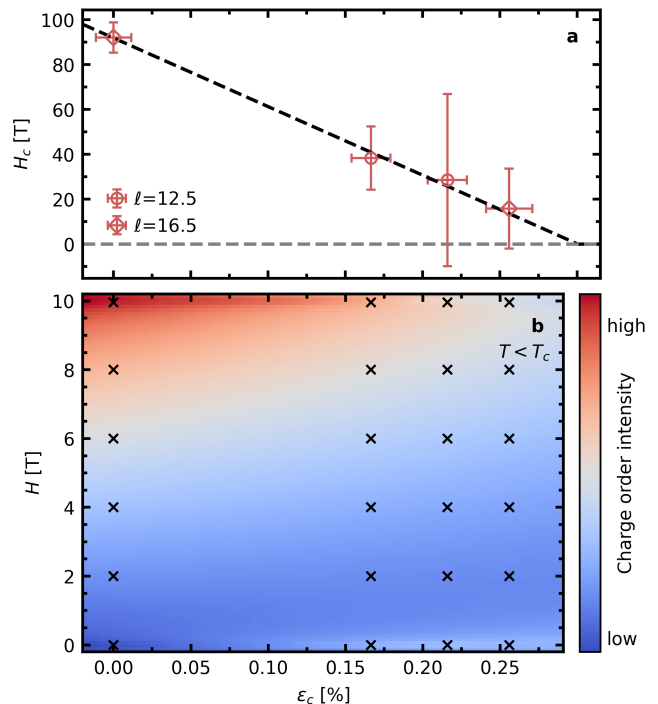


FIG. 4. **Magnetic field and strain effects.** **a** The magnetic field scale H_c versus compressive c -axis strain ϵ_c at 10 K. Data points were obtained from measurements and fits of charge order peaks at $(0.231, \ell)$ with $\ell = 12.5, 16.5$. Vertical error bars are Gaussian standard deviations from fits to the magnetic field dependence of the charge order reflection. Horizontal error bars reflect uncertainty of the strain estimation. The black dashed line is a linear guide to the eye **b** Schematic illustration of the magnetic field H and strain effect on the charge order peak amplitude inside the superconducting state. We expect – by extrapolation – the magnetic field enhancement to fully vanish. Crosses display the phase space covered by our experiments.

three different growth cycles – all with nominal strontium content of $x \approx 0.12$. The effective strontium contents were gauged from magnetic susceptibility measurements of the superconducting transition temperature. All x-ray diffraction data in the main text stem from batch I – see Table I. For the a -axis, pointing approximately along the (transmitted) x-ray beam direction, the ideal sample thickness L_a matches the half-value thickness ($d_{1/2} \sim 0.63$ mm for LSCO [43, 44]). At this trade-off point ($L_a \approx d_{1/2}$), half of the incident x-ray flux is transmitted through the sample. We optimized L_a for the XRD experiments, so that $L_a \approx d_{1/2}$ (see Fig. 1a and Table 1).

X-Ray Diffraction and Pressure Cell

Hard x-ray diffraction experiments were carried out at the P21.1 beamline at PETRA III (DESY, Hamburg)

synchrotron using 101.6 keV photons. All measurements were performed with a Dectris Pilatus 100K CdTe detector. Uniaxial pressure and magnetic field were applied along the crystallographic c -axis. Misalignment of c -axis and press direction is no more than 4° . As such, unintentional in-plane pressure application is negligible [27]. In the absence of a magnetic field, a standard (ex-situ) screw cell was used [27, 45]. An adaption was made to fit into a horizontal magnet [29, 32] with pressure application parallel to the direction of the magnetic field. The designs of the two uniaxial pressure cells are shown in Supplementary Fig. 5 a, b. For both cells, the horizontal scattering plane is spanned by a copper-oxygen bond direction and the c -axis. This gives access to the $(h, 0, \ell)$ reciprocal plane. Consistent results are obtained with both setups (displex and cryomagnet) – see Supplementary Fig. 6. Throughout the manuscript, reciprocal space vectors (h, k, ℓ) are given in units of $(\frac{2\pi}{a}, \frac{2\pi}{b}, \frac{2\pi}{c})$ with $a = b \approx 3.77 \text{ \AA}$ and $c \approx 13.2 \text{ \AA}$. Notice that even though LSCO has a low-temperature orthorhombic crystal structure with a and b axes at 45 degrees to the Cu-O bonds with twin domains [27, 46–48], the stripe ordering vector is traditionally expressed in tetragonal notation. The magnitude of applied strain is determined from measurements of Bragg reflections, similar to what is described by Choi et al. [27]. Bragg peak intensities are only marginally affected by the application of pressure (see Supplementary Fig. 7 and Supplementary Tab. 1). We defined the zero-strain, low-temperature lattice parameter as c_0 and c -axis strain as $\varepsilon_c = (c_0 - c)/c_0$. Both c_0 and c are determined from Bragg peaks of the type $(0, 0, \pm n)$ with n being an even integer (see Fig. 1b). Using this methodology a calibration curve between screw turn and strain is established (see Supplementary Fig. 4). Compressive c -axis strain induces – with Poisson’s ratio of ≈ 0.3 [37] – tensile strains along the a - and b -directions. Notice that this is different from compressive b -axis strain [27] that generates tensile strain along the a - and c -axes directions, again with Poisson’s ratio.

Neutron Diffraction

Neutron diffraction data were measured at the TASP spectrometer at SINQ, PSI on LSCO $x = 0.115$ ($T_c \approx 27 \text{ K}$). The sample in the (ex-situ) pressure cell was mounted in a coil (see Supplementary Fig. 5c), custom-built to fit inside a cryostat, which itself was mounted inside the Mu-metal polarization analysis device MuPAD [49]. The sample was cooled from 40 K to 10 K in a magnetic field of 30 G, applied along the crystallographic c -direction, perpendicular to the scattering plane. At base temperature, the field was subsequently turned off. Using MuPAD’s spherical polarimetry capabilities, a full polarization matrix was measured on the in-plane Bragg peak $\tau = (-1, -1, 0)$.

The highest flipping ratio of 6.87 was found for neutron polarization along y (in the scattering plane but perpendicular to τ). The temperature dependence of the intensity of $\tau = (-1, -1, 0)$ was tracked in the Py- y spin flip channel upon slowly heating. The flux trapped along the c -direction during the field-cooling procedure gives rise to an excess depolarization of the neutron beam, which is reflected in an increased spin-flip intensity. Upon crossing T_c , the trapped flux is released. Intensities are normalized to the monitor and scaled by the integrated Bragg peak of $(-1, -1, 0)$ in unstrained LSCO. To extract the transition temperature, spin flip intensities were fitted with $p_0 \cdot \tanh(T - T_c) + p_1$. The resulting T_c of the zero-pressure LSCO crystal is in accord with the transition temperature obtained from a magnetic susceptibility measurement of the rod (see Supplementary Fig. 8).

Data availability. Data are available upon request.

Code availability. Code is available upon request.

Competing interests. The authors declare no competing interests.

Acknowledgements: J.K., R.F., L.M., D.B., and J.C. acknowledge support from the Swiss National Science Foundation (Projects No. 200021_188564 and No. 200021_296 185037). J.K. is further supported by the PhD fellowship from the German Academic Scholarship Foundation. I.B. acknowledges support from the Swiss Government Excellence Scholarship. Q.W. is supported by the Research Grants Council of Hong Kong (ECS No. 24306223), and the CUHK Direct Grant (No. 4053613). N.B.C. was supported by the Danish National Council for Research infrastructure (NUFI) through DANSCATT and the ESS-Lighthouse Q-MAT. This research was carried out at beamline P21.1 at DESY, a member of the Helmholtz Association (HGF). We would like to thank Philipp Glaevecke for technical assistance during the experiment. The research leading to this result has been supported by the project CALIPSOplus under the Grant Agreement 730872 from the EU Framework Programme for Research and Innovation HORIZON 2020. Part of the research have been carried out at the TASP endstation of the spallation source SINQ (PSI).

Authors Contribution: TK, NM, MO grew and JK prepared the LSCO crystals. JChoi, DB, MJ designed and tested the pressure cells. X-ray diffraction experiments were carried out by JK, RF, AM, OI, MvZ, NBC, QW, JChang. Polarized neutron scattering experiments were conducted by JK, NBC, DGM, GS, AAT, LT, DWT. JK carried out the data analysis with input from IB, QW, and LM. The project was conceived by JK and JChang who also wrote the manuscript with input from all authors.

Crystal Batch	T_c [K]	$L_a \cdot L_b \cdot L_c$ [mm ³]	Figure
I	27	0.5 · 1.4 · 1.4	1b,d 2, 3, 4 Supplementary Fig. 1, 3, 4, 6, 7
II	27	0.8 · 1.0 · 1.5	1c Supplementary Fig. 8
III	30	0.7 · 0.7 · 1.2	Supplementary Fig. 2

TABLE I. **Sample dimensions.** Samples from three different batches were cut along the two Cu-O directions and the c -axis – defining three lengths: L_a , L_b , and L_c (see Fig. 1a). The last column indicates the figures which contain data taken on a given sample.

REFERENCES

- * julia.kuespert@physik.uzh.ch
† qwang@cuhk.edu.hk
- [1] D. Gibbs, K. M. Mohanty, and J. Bohr, High-resolution x-ray-scattering study of charge-density-wave modulation in chromium, *Phys. Rev. B* **37**, 562 (1988).
 - [2] X. W. Jiang and R. S. Fishman, Coupled spin- and charge-density waves in chromium alloys, *Journal of Physics: Condensed Matter* **9**, 3417 (1997).
 - [3] Y. Hu, T. Zhang, D. Zhao, C. Chen, S. Ding, W. Yang, X. Wang, C. Li, H. Wang, D. Feng, and T. Zhang, Real-space observation of incommensurate spin density wave and coexisting charge density wave on Cr (001) surface, *Nature Communications* **13**, 445 (2022).
 - [4] J. M. Tranquada, D. J. Buttrey, V. Sachan, and J. E. Lorenzo, Simultaneous ordering of holes and spins in $\text{La}_2\text{NiO}_{4.125}$, *Phys. Rev. Lett.* **73**, 1003 (1994).
 - [5] J. M. Tranquada, J. D. Axe, N. Ichikawa, Y. Nakamura, S. Uchida, and B. Nachumi, Neutron-scattering study of stripe-phase order of holes and spins in $\text{La}_{1.48}\text{Nd}_{0.4}\text{Sr}_{0.12}\text{CuO}_4$, *Phys. Rev. B* **54**, 7489 (1996).
 - [6] M. Hücker, M. v. Zimmermann, G. D. Gu, Z. J. Xu, J. S. Wen, G. Xu, H. J. Kang, A. Zheludev, and J. M. Tranquada, Stripe order in superconducting $\text{La}_{2-x}\text{Ba}_x\text{CuO}_4$ ($0.095 \leq x \leq 0.155$), *Phys. Rev. B* **83**, 104506 (2011).
 - [7] V. Thampy, M. P. M. Dean, N. B. Christensen, L. Steinke, Z. Islam, M. Oda, M. Ido, N. Momono, S. B. Wilkins, and J. P. Hill, Rotated stripe order and its competition with superconductivity in $\text{La}_{1.88}\text{Sr}_{0.12}\text{CuO}_4$, *Phys. Rev. B* **90**, 100510(R) (2014).
 - [8] A. J. Achkar, M. Zwiebler, C. McMahan, F. He, R. Surtarto, I. Djianto, Z. Hao, M. J. P. Gingras, M. Hücker, G. D. Gu, A. Revcolevschi, H. Zhang, Y.-J. Kim, J. Geck, and D. G. Hawthorn, Nematicity in stripe-ordered cuprates probed via resonant x-ray scattering, *Science* **351**, 576 (2016).
 - [9] F. H. Yu, D. H. Ma, W. Z. Zhuo, S. Q. Liu, X. K. Wen, B. Lei, J. J. Ying, and X. H. Chen, Unusual competition of superconductivity and charge-density-wave state in a compressed topological kagome metal, *Nature Communications* **12**, 3645 (2021).
 - [10] Y. Song, T. Ying, X. Chen, X. Han, X. Wu, A. P. Schnyder, Y. Huang, J.-g. Guo, and X. Chen, Competition of superconductivity and charge density wave in selective oxidized CsV_3Sb_5 thin flakes, *Phys. Rev. Lett.* **127**, 237001 (2021).
 - [11] S. Nandi, M. G. Kim, A. Kreyssig, R. M. Fernandes, D. K. Pratt, A. Thaler, N. Ni, S. L. Bud'ko, P. C. Canfield, J. Schmalian, R. J. McQueeney, and A. I. Goldman, Anomalous suppression of the orthorhombic lattice distortion in superconducting $\text{Ba}(\text{Fe}_{1-x}\text{Co}_x)_2\text{As}_2$ single crystals, *Phys. Rev. Lett.* **104**, 057006 (2010).
 - [12] D. Hu, D. W. Tam, W. Zhang, Y. Wei, R. Georgii, B. Pedersen, A. C. Roldan, and P. Dai, Uniaxial c -axis pressure effects on the underdoped superconductor $\text{BaFe}_2(\text{As}_{0.72}\text{P}_{0.28})_2$, *Phys. Rev. B* **101**, 020507 (2020).
 - [13] J. M. Allred, K. M. Taddei, D. E. Bugaris, S. Avci, D. Y. Chung, H. Claus, C. dela Cruz, M. G. Kanatzidis, S. Rosenkranz, R. Osborn, and O. Chmaissem, Coincident structural and magnetic order in $\text{bafe}_2(\text{As}_{1-x}\text{P}_x)_2$ revealed by high-resolution neutron diffraction, *Phys. Rev. B* **90**, 104513 (2014).
 - [14] J. Flouquet, D. Aoki, F. Bourdarot, F. Hardy, E. Hassinger, G. Knebel, T. D. Matsuda, C. Meingast, C. Paulsen, and V. Taufour, Trends in heavy fermion matter, *Journal of Physics: Conference Series* **273**, 012001 (2011).
 - [15] D. F. Agterberg, J. S. Davis, S. D. Edkins, E. Fradkin, D. J. V. Harlingen, S. A. Kivelson, P. A. Lee, L. Radzihovsky, J. M. Tranquada, and Y. Wang, The physics of pair-density waves: Cuprate superconductors and beyond, *Annual Review of Condensed Matter Physics* **11**, 231 (2020).
 - [16] Y. Wang, S. D. Edkins, M. H. Hamidian, J. C. S. Davis, E. Fradkin, and S. A. Kivelson, Pair density waves in superconducting vortex halos, *Phys. Rev. B* **97**, 174510 (2018).
 - [17] Z. Dai, Y.-H. Zhang, T. Senthil, and P. A. Lee, Pair-density waves, charge-density waves, and vortices in high- T_c cuprates, *Phys. Rev. B* **97**, 174511 (2018).
 - [18] J. M. Tranquada, B. J. Sternlieb, J. D. Axe, Y. Nakamura, and S. Uchida, Evidence for stripe correlations of spins and holes in copper oxide superconductors, *Nature (London)* **375**, 561 (1995).
 - [19] T. P. Croft, C. Lester, M. S. Senn, A. Bombardi, and S. M. Hayden, Charge density wave fluctuations in $\text{La}_{2-x}\text{Sr}_x\text{CuO}_4$ and their competition with superconductivity, *Phys. Rev. B* **89**, 224513 (2014).
 - [20] E. Pavarini, I. Dasgupta, T. Saha-Dasgupta, O. Jepsen, and O. K. Andersen, Band-structure trend in hole-doped cuprates and correlation with $T_{c\text{max}}$, *Phys. Rev. Lett.* **87**, 047003 (2001).
 - [21] F. Gugenberger, C. Meingast, G. Roth, K. Grube, V. Breit, T. Weber, H. Wühl, S. Uchida, and Y. Nakamura, Uniaxial pressure dependence of t_c from high-resolution dilatometry of untwinned $\text{La}_{2-x}\text{Sr}_x\text{CuO}_4$ single crystals, *Phys. Rev. B* **49**, 13137 (1994).
 - [22] A. Jalekeshov and B. Yavidov, On the uniaxial strain (pressure) derivatives of the critical temperature of superconductivity of $\text{La}_{2-x}\text{Sr}_x\text{CuO}_4$, *Physica C: Supercon-*

- ductivity and its Applications **604**, 1354177 (2023).
- [23] F. Nakamura, J. Hori, T. Goko, Y. Uno, N. Kikugawa, and T. Fujita, T_c enhancement in $\text{La}_{2-x}\text{Sr}_x\text{CuO}_4$ under anisotropic pressure, *Journal of Low Temperature Physics* **117**, 1145 (1999).
- [24] H. Sato and M. Naito, Increase in the superconducting transition temperature by anisotropic strain effect in (001) $\text{La}_{1.85}\text{Sr}_{0.15}\text{CuO}_4$ thin films on LaSrAlO_4 substrates, *Physica C: Superconductivity* **274**, 221 (1997).
- [25] J. Locquet and E. Williams, Epitaxially Induced Defects in Sr- and O-doped La_2CuO_4 Thin Films Grown by MBE: Implications for Transport Properties, *Acta Phys. Pol. A* **92**, 69–84 (1997).
- [26] N. Takeshita, T. Sasagawa, T. Sugioka, Y. Tokura, and H. Takagi, Gigantic anisotropic uniaxial pressure effect on superconductivity within the CuO_2 plane of $\text{La}_{1.64}\text{Eu}_{0.2}\text{Sr}_{0.16}\text{CuO}_4$: Strain control of stripe criticality, *Journal of the Physical Society of Japan* **73**, 1123 (2004).
- [27] J. Choi, Q. Wang, S. Jöhr, N. B. Christensen, J. Küspert, D. Bucher, D. Biscette, M. H. Fischer, M. Hücker, T. Kurosawa, N. Momono, M. Oda, O. Ivashko, M. v. Zimmermann, M. Janoschek, and J. Chang, Unveiling unequivocal charge stripe order in a prototypical cuprate superconductor, *Phys. Rev. Lett.* **128**, 207002 (2022).
- [28] E. Demler, S. Sachdev, and Y. Zhang, Spin-ordering quantum transitions of superconductors in a magnetic field, *Phys. Rev. Lett.* **87**, 067202 (2001).
- [29] N. B. Christensen, J. Chang, J. Larsen, M. Fujita, M. Oda, M. Ido, N. Momono, E. M. Forgan, A. T. Holmes, J. Mesot, M. Huecker, and M. v. Zimmermann, Bulk charge stripe order competing with superconductivity in $\text{La}_{2-x}\text{Sr}_x\text{CuO}_4$ ($x = 0.12$), [arXiv:1404.3192](https://arxiv.org/abs/1404.3192) (2014).
- [30] J. Chang, C. Niedermayer, R. Gilardi, N. B. Christensen, H. M. Rønnow, D. F. McMorrow, M. Ay, J. Stahn, O. Sobolev, A. Hiess, S. Pailhes, C. Baines, N. Momono, M. Oda, M. Ido, and J. Mesot, Tuning competing orders in $\text{La}_{2-x}\text{Sr}_x\text{CuO}_4$ cuprate superconductors by the application of an external magnetic field, *Phys. Rev. B* **78**, 104525 (2008).
- [31] B. Lake, H. M. Rønnow, N. B. Christensen, G. Aeppli, K. Lefmann, D. F. McMorrow, P. Vorderwisch, P. Smeibidl, N. Mangkorntong, T. Sasagawa, M. Nohara, H. Takagi, and T. E. Mason, Antiferromagnetic order induced by an applied magnetic field in a high-temperature superconductor, *Nature* **415**, 299 (2002).
- [32] M. Hücker, M. v. Zimmermann, Z. J. Xu, J. S. Wen, G. D. Gu, and J. M. Tranquada, Enhanced charge stripe order of superconducting $\text{La}_{2-x}\text{Ba}_x\text{CuO}_4$ in a magnetic field, *Phys. Rev. B* **87**, 014501 (2013).
- [33] B. Khaykovich, S. Wakimoto, R. J. Birgeneau, M. A. Kastner, Y. S. Lee, P. Smeibidl, P. Vorderwisch, and K. Yamada, Field-induced transition between magnetically disordered and ordered phases in underdoped $\text{La}_{2-x}\text{Sr}_x\text{CuO}_4$, *Phys. Rev. B* **71**, 220508 (2005).
- [34] J.-J. Wen, W. He, H. Jang, H. Nojiri, S. Matsuzawa, S. Song, M. Chollet, D. Zhu, Y.-J. Liu, M. Fujita, J. M. Jiang, C. R. Rotundu, C.-C. Kao, H.-C. Jiang, J.-S. Lee, and Y. S. Lee, Enhanced charge density wave with mobile superconducting vortices in $\text{La}_{1.885}\text{Sr}_{0.115}\text{CuO}_4$, *Nature Communications* **14**, 733 (2023).
- [35] B. Lake, G. Aeppli, K. N. Clausen, D. F. McMorrow, K. Lefmann, N. E. Hussey, N. Mangkorntong, M. Nohara, H. Takagi, T. E. Mason, and A. Schröder, Spins in the vortices of a high-temperature superconductor, *Science* **291**, 1759 (2001).
- [36] T. Wu, H. Mayaffre, S. Krämer, M. Horvatić, C. Berthier, P. L. Kuhns, A. P. Reyes, R. Liang, W. N. Hardy, D. A. Bonn, and M.-H. Julien, Emergence of charge order from the vortex state of a high-temperature superconductor, *Nature Communications* **4**, 2113 (2013).
- [37] F. Nakamura, T. Goko, J. Hori, Y. Uno, N. Kikugawa, and T. Fujita, Role of two-dimensional electronic state in superconductivity in $\text{La}_{2-x}\text{Sr}_x\text{CuO}_4$, *Phys. Rev. B* **61**, 107 (2000).
- [38] C. E. Matt, D. Sutter, A. M. Cook, Y. Sassa, M. Månsson, O. Tjernberg, L. Das, M. Horio, D. De-straz, C. G. Fatuzzo, K. Hauser, M. Shi, M. Kobayashi, V. N. Strocov, T. Schmitt, P. Dudin, M. Hoesch, S. Pyon, T. Takayama, H. Takagi, O. J. Lipscombe, S. M. Hayden, T. Kurosawa, N. Momono, M. Oda, T. Neupert, and J. Chang, Direct observation of orbital hybridisation in a cuprate superconductor, *Nat. Commun.* **9**, 972 (2018).
- [39] K. P. Kramer, M. Horio, S. S. Tsirkin, Y. Sassa, K. Hauser, C. E. Matt, D. Sutter, A. Chikina, N. B. M. Schröter, J. A. Krieger, T. Schmitt, V. N. Strocov, N. C. Plumb, M. Shi, S. Pyon, T. Takayama, H. Takagi, T. Adachi, T. Ohgi, T. Kawamata, Y. Koike, T. Kondo, O. J. Lipscombe, S. M. Hayden, M. Ishikado, H. Eisaki, T. Neupert, and J. Chang, Band structure of overdoped cuprate superconductors: Density functional theory matching experiments, *Phys. Rev. B* **99**, 224509 (2019).
- [40] H. Sakakibara, H. Usui, K. Kuroki, R. Arita, and H. Aoki, Two-Orbital Model Explains the Higher Transition Temperature of the Single-Layer Hg-Cuprate Superconductor Compared to That of the La-Cuprate Superconductor, *Phys. Rev. Lett.* **105**, 057003 (2010).
- [41] H. Sakakibara, H. Usui, K. Kuroki, R. Arita, and H. Aoki, Origin of the material dependence of T_c in the single-layered cuprates, *Phys. Rev. B* **85**, 064501 (2012).
- [42] Y. Koike, T. Adachi, Y. Tanabe, K. Omori, T. Noji, and H. Sato, Inhomogeneous superconductivity in both underdoped and overdoped regimes of high- T_c cuprates, *Journal of Physics: Conference Series* **108**, 012003 (2008).
- [43] B. P. and C. Segre, (2020), accessed: 2024-02-06.
- [44] W. H. McMaster, N. K. del Grande, J. H. Mallett, and J. H. Hubbell, Compilation of x-ray cross sections ucrl-50174, sections i, ii revision 1, iii, iv*, Lawrence Livermore National Laboratory Report UCRL-50174 (section I 1970, section II 1969, section III 1969 and section IV 1969) (1970).
- [45] G. Simutis, J. Küspert, Q. Wang, J. Choi, D. Bucher, M. Boehm, F. Bourdarot, M. Bertelsen, C. N. Wang, T. Kurosawa, N. Momono, M. Oda, M. Månsson, Y. Sassa, M. Janoschek, N. B. Christensen, J. Chang, and D. G. Mazzone, Single-domain stripe order in a high-temperature superconductor, *Communications Physics* **5**, 296 (2022).
- [46] H. Jacobsen, I. A. Zaliznyak, A. T. Savici, B. L. Winn, S. Chang, M. Hücker, G. D. Gu, and J. M. Tranquada, Neutron scattering study of spin ordering and stripe pinning in superconducting $\text{La}_{1.93}\text{Sr}_{0.07}\text{CuO}_4$, *Phys. Rev. B* **92**, 174525 (2015).
- [47] Y. Horibe, Y. Inoue, and Y. Koyama, Direct observation of dynamic local structure in $\text{La}_{2-x}\text{Sr}_x\text{CuO}_4$ around $x =$

- 0.12, [Phys. Rev. B **61**, 11922 \(2000\)](#).
- [48] R. Frison, J. Küspert, Q. Wang, O. Ivashko, M. v. Zimmermann, M. Meven, D. Bucher, J. Larsen, C. Niedermayer, M. Janoschek, T. Kurosawa, N. Momono, M. Oda, N. B. Christensen, and J. Chang, Crystal symmetry of stripe-ordered $\text{La}_{1.88}\text{Sr}_{0.12}\text{CuO}_4$, [Phys. Rev. B **105**, 224113 \(2022\)](#).
- [49] M. Janoschek, S. Klimko, R. Gähler, B. Roessli, and P. Böni, Spherical neutron polarimetry with mupad, [Physica B: Condensed Matter **397**, 125 \(2007\)](#).

Supplementary Material for Engineering Phase Competition Between Stripe Order and Superconductivity in $\text{La}_{1.88}\text{Sr}_{0.12}\text{CuO}_4$

J. Küspert,^{1,*} I. Bialo,^{1,2} R. Frison,¹ A. Morawietz,¹ L. Martinelli,¹ J. Choi,³ D. Bucher,¹ O. Ivashko,⁴ M. v. Zimmermann,⁴ N. B. Christensen,⁵ D. G. Mazzone,⁶ G. Simutis,⁷ A. A. Turrini,⁶ L. Thomarat,^{7,8} D. W. Tam,⁶ M. Janoschek,^{1,7} T. Kurosawa,⁹ N. Momono,^{9,10} M. Oda,⁹ Qisi Wang,^{1,11,†} and J. Chang¹

¹Physik-Institut, Universität Zürich, Winterthurerstrasse 190, CH-8057 Zürich, Switzerland

²AGH University of Krakow, Faculty of Physics and Applied Computer Science, 30-059 Krakow, Poland

³Diamond Light Source, Harwell Campus, Didcot OX11 0DE, United Kingdom

⁴Deutsches Elektronen-Synchrotron DESY, Notkestraße 85, 22607 Hamburg, Germany

⁵Department of Physics, Technical University of Denmark, DK-2800 Kongens Lyngby, Denmark

⁶Laboratory for Neutron Scattering and Imaging,
Paul Scherrer Institut, CH-5232, Villigen-PSI, Switzerland

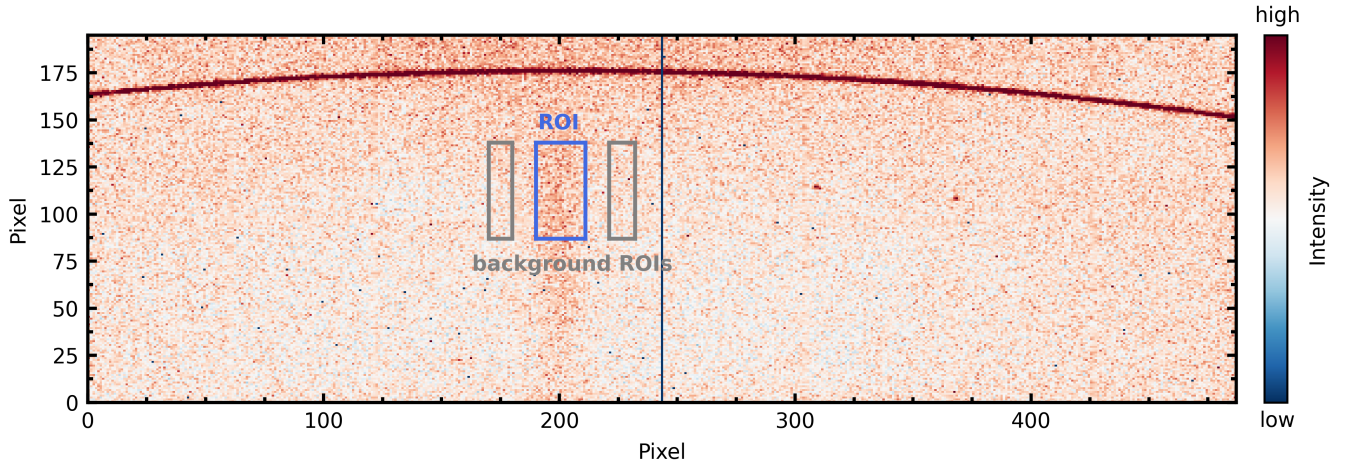
⁷Laboratory for Neutron and Muon Instrumentation,
Paul Scherrer Institut, CH-5232 Villigen PSI, Switzerland

⁸École normale supérieure Paris-Saclay, 91190 Gif-sur-Yvette, France

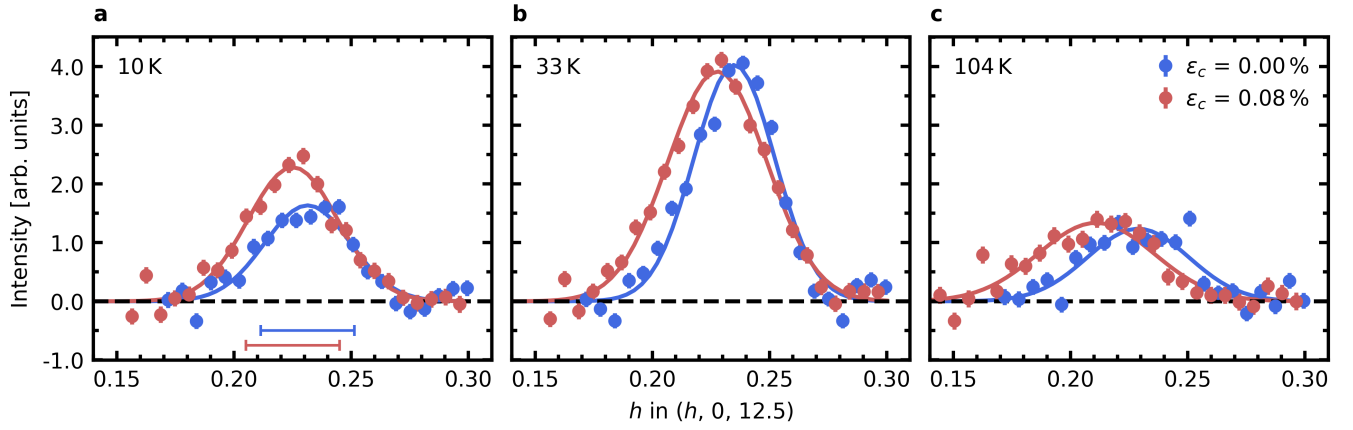
⁹Department of Physics, Hokkaido University, Sapporo 060-0810, Japan

¹⁰Department of Applied Sciences, Muroran Institute of Technology, Muroran 050-8585, Japan

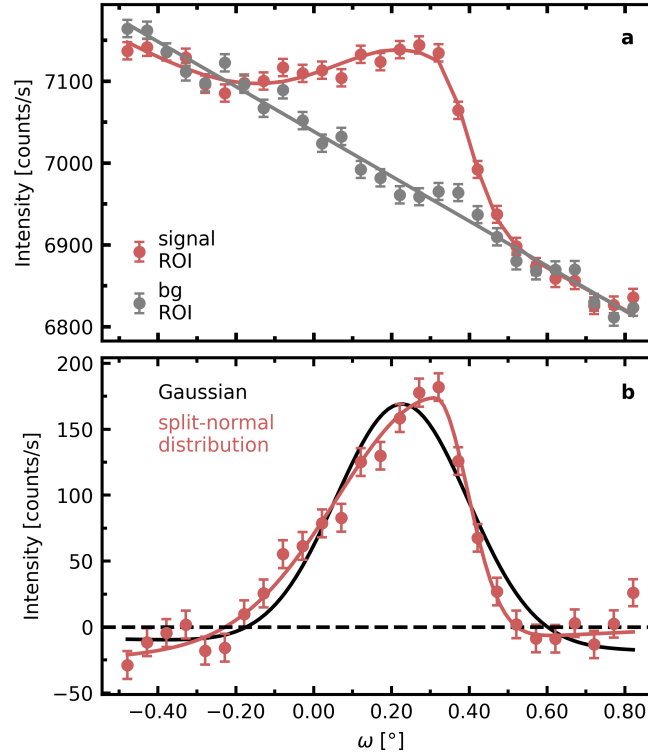
¹¹Department of Physics, The Chinese University of Hong Kong, Shatin, Hong Kong, China



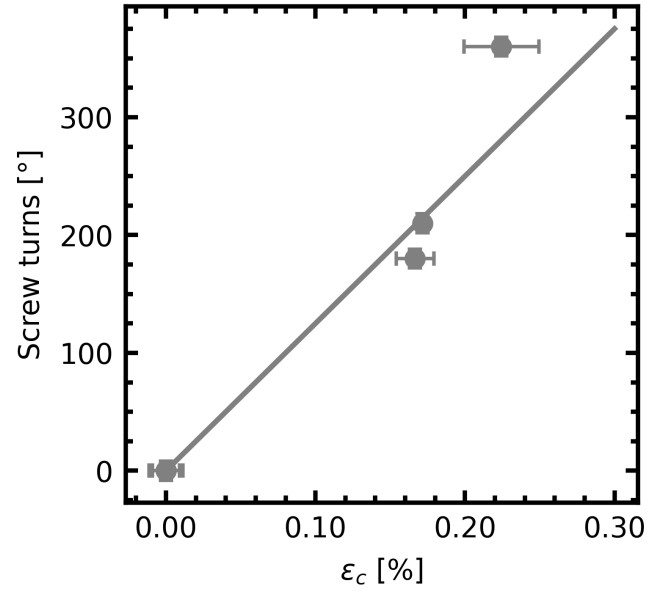
Supplementary Figure 1. Example of detector image. 2D detector image recorded on LSCO $x = 12\%$ ($T_c = 27\text{K}$) and displayed with false color scale. Signal region-of-interest (ROI) around $\mathbf{Q}_{\text{co}} = (0.231, 0, 12.5)$ and background ROIs are indicated by respectively blue and grey rectangles. The most intense feature running horizontally across the detector is a powder line stemming from the sample environment. The vertical line is a gap between two parts of the detector.



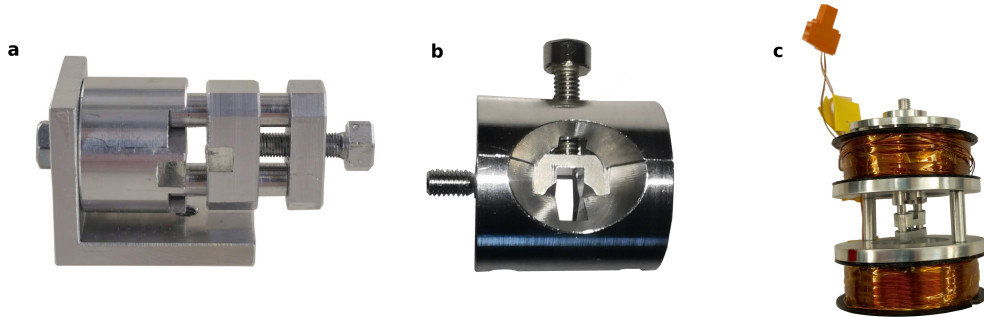
Supplementary Figure 2. Charge order reflection recorded on LSCO ($T_c = 30$ K, $x = 12.5$ %) upon application of c -axis uniaxial strain. a-c Background subtracted intensity along $Q_{co} = (h, 0, 12.5)$ for temperature and strain conditions as indicated. Vertical error bars represent counting statistics. Horizontal lines in (a) – applying to all panels – account for a systematic error in momentum determination.



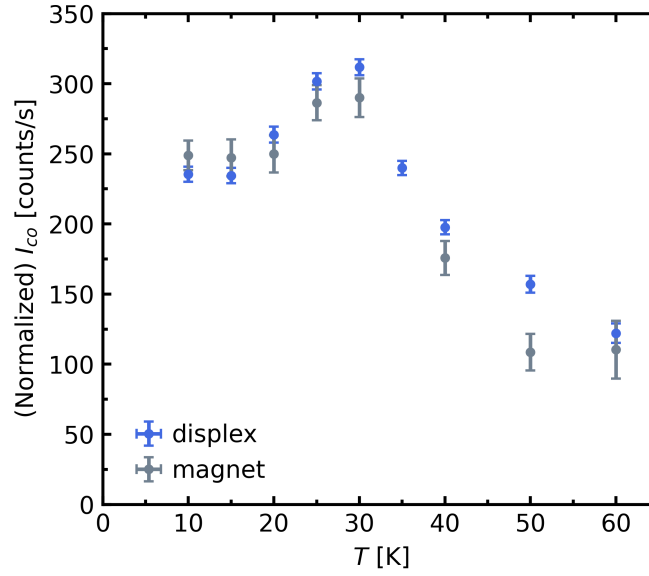
Supplementary Figure 3. Comparison of fit functions for the charge order peak at $Q_{co} = (0.231, 0, 12.5)$. **a** Intensity from rocking scans through the charge order reflection and corresponding background obtained from integration of "signal" and "background" ROIs (see Supplementary Fig. 1). The sample was exposed to an uniaxial strain of $\epsilon_c = (0.17 \pm 0.01)$ %, measured by the experimental setup using a cryomagnet at 30 K. **b** Background subtracted intensities for the rocking scan shown in a. Solid black and red lines are respectively fits to a Gaussian function and a split-normal distribution. The resulting amplitudes are (182.99 ± 6.00) counts/s and (184.94 ± 5.95) counts/s, respectively. Thus within error bars, the amplitude is independent of the two fit functions. As the split-normal distribution provides a better fit, this function is consistently used in our analysis. To be specific, a split-normal distribution with linear background is defined as: $I(\omega) = I_{co} \cdot \exp(-(\omega - \omega_0)^2 / (2\sigma^2)) + b_1\omega + b_0$, where $\sigma = \sigma_1$ if $\omega \leq \omega_0$ and $\sigma = \sigma_2$ if $\omega > \omega_0$. σ is the width of the function, ω_0 its peak position, I_{co} the amplitude, and b_1 and b_0 fitting parameters defining the background. Error bars are set by counting statistics.



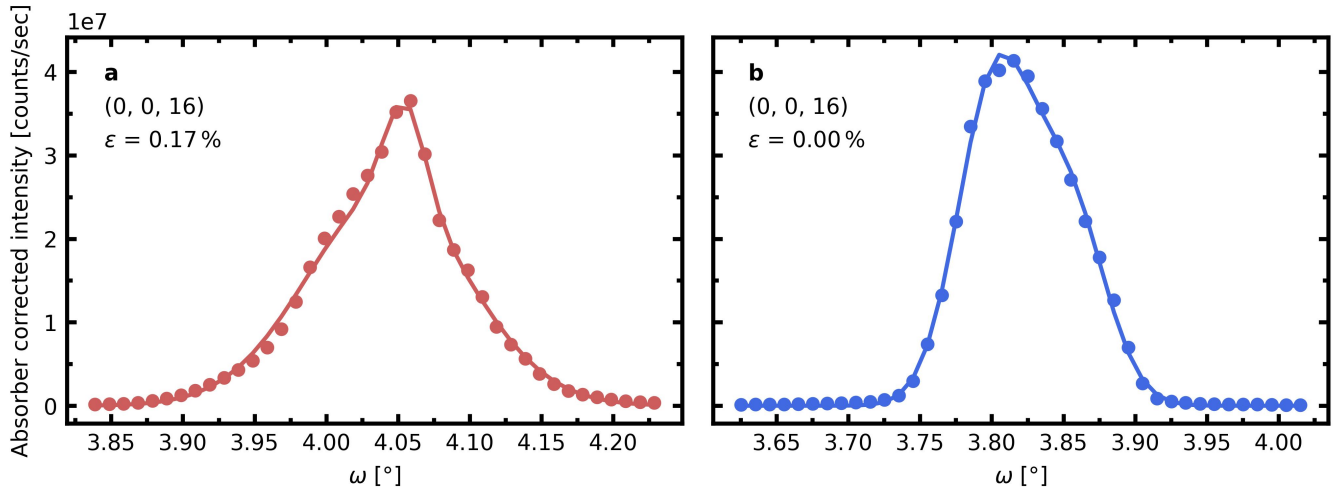
Supplementary Figure 4. Strain calibration curve. Pressure cell screw turns (st) versus strain $\epsilon_c = (c - c_0)/c_0$, where c_0 is the unstrained c -axis lattice parameter and c is the strained lattice parameter. c_0 and c are determined as described in the Methods section. The solid line is a linear fit of the form $st = m \cdot \epsilon_c$, with m being a fit parameter. Vertical errors reflect precision in screw turns ($\pm 8^\circ$), while horizontal errors are derived from standard deviations obtained from the fitting.



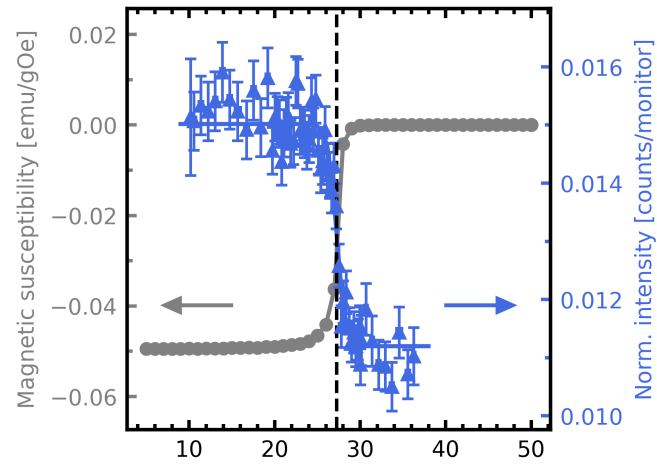
Supplementary Figure 5. Strain cells for c -axis strain application. **a** Strain cell for experimental setup without magnetic field (displex cryo-environment). We extended the strain cell used in [1] with an adapter to apply strain in c -axis direction while having a - and c -axis in the horizontal scattering plane. **b** Strain cell for experiment with a cryomagnet. The design is more compact in order to fit into the magnet bore. **c** Strain cell from a (without adapter) inside the coil to be mounted inside the MuPad [2] for the neutron experiment.



Supplementary Figure 6. Temperature dependence of charge order amplitude in different experimental environments. Both data sets stem from the same unstrained LSCO sample. Blue data were measured in the displex on an Euler cradle, while grey data were measured in a cryomagnet. Error bars are standard deviations from fitting of charge order peak.



Supplementary Figure 7. Comparison of Bragg peaks upon application of pressure. **a** Bragg peak at $(0, 0, 16)$ with $\epsilon_c = 0.17\%$. **b** Same Bragg peak in ambient pressure conditions, after strain was released from the sample. Solid lines are guides to the eye. Error bars stem from counting statistics. Notice that errors are smaller than the point size and hence invisible.



Supplementary Figure 8. Comparison of (zero-pressure) superconducting transition temperature determined from zero-field-cooled DC magnetic susceptibility (grey, left) and polarized neutron scattering (blue, right). Error bars of neutron diffraction data represent counting statistics.

Sample Environment	Crystal Batch	$(0, 0, n)$	$(I_{int}^{0.00\%} - I_{int}^{0.17\%}) / (I_{int}^{0.00\%} + I_{int}^{0.17\%})$	$I_{int}^{0.00\%} / I_{int}^{0.17\%}$
displex	I	$(0, 0, 4)$	0.126 ± 0.006	1.29 ± 0.05
magnet cryostat	I	$(0, 0, 4)$	-0.041 ± 0.003	0.92 ± 0.06
displex	I	$(0, 0, -12)$	-0.01 ± 0.01	1.0 ± 0.1
displex	I	$(0, 0, 12)$	-0.01 ± 0.01	1.0 ± 0.1
magnet cryostat	I	$(0, 0, -8)$	-0.036 ± 0.003	0.93 ± 0.06
magnet cryostat	I	$(0, 0, 16)$	0.004 ± 0.002	1.01 ± 0.06

Supplementary Table 1. Comparison of Bragg peak intensities. Ratios $(I_{int}^{0.00\%} - I_{int}^{0.17\%}) / (I_{int}^{0.00\%} + I_{int}^{0.17\%})$ and $I_{int}^{0.00\%} / I_{int}^{0.17\%}$ for the two different sample environments, including the Bragg peaks in Fig. 7. I_{int} is the integrated intensity and the superscript indicates the strain. All values bear upon $(0, 0, n)$ as indicated and the sample of batch I (see Tab. 1). Integration is performed using the composite trapezoidal rule. Errors stem from biggest error estimation with the errors of the summed intensity of the ROI and Gaussian error propagation.

SUPPLEMENTARY REFERENCES

* julia.kuespert@physik.uzh.ch

† qwang@cuhk.edu.hk

- [1] J. Choi, Q. Wang, S. Jöhr, N. B. Christensen, J. Küspert, D. Bucher, D. Biscette, M. H. Fischer, M. Hücker, T. Kurosawa, N. Momono, M. Oda, O. Ivashko, M. v. Zimmermann, M. Janoschek, and J. Chang, Unveiling unequivocal charge stripe order in a prototypical cuprate superconductor, *Phys. Rev. Lett.* **128**, 207002 (2022).
- [2] M. Janoschek, S. Klimko, R. Gähler, B. Roessli, and P. Böni, Spherical neutron polarimetry with mupad, *Physica B: Condensed Matter* **397**, 125 (2007).